Is Infrared Laser-Induced Desorption a Thermal Process? The Case of Aniline

Martin Handschuh, Stefan Nettesheim, and Renato Zenobi*

Department of Chemistry, ETH Zentrum, Universitätsstr. 16, CH-8092 Zürich, Switzerland

Received: October 22, 1998

A complete study of nanosecond laser-induced thermal desorption (LITD) of aniline submonolayers from silica as well as nanosecond and picosecond laser desorption from glassy graphite was undertaken. The measurements include determination of equilibrium desorption kinetic parameters; time-resolved studies on the surface temperature and the surface coverage during laser heating; and investigation of translational, vibrational, and rotational temperatures of laser-desorbed molecules. Our findings are that LITD of aniline up to heating rates of 10^{10} K/s is consistent with complete thermalization of the molecules during fast desorption. At 10^{13} K/s, only the kinetic energy of the desorbed molecules agrees well with a thermal desorption model, whereas the internal degrees of freedom are not fully equilibrated, but appear to be somewhat colder.

Introduction

A basic requirement for mass analysis by desorption−ionization methods is that the desorption process should release intact analyte molecules from the sample. In this respect, laser desorption is by far the most successful of many desorption techniques available, providing access to intact gas-phase molecules from high molecular weight, polar, nonvolatile, and thermally labile sample materials.[1−6] For mass spectrometric analysis, ions are either generated by the same laser pulse (for example, in matrix-assisted laser desorption/ionization[3,4]) or by the uses of a postionization step.[7,8] Two techniques are commonly used to desorb adsorbates from substrates: resonant laser desorption by direct vibrational[9,10] or electronic[11,12] excitation of the adsorbates or laser-induced thermal desorption (LITD) by indirect heating of the substrate. Desorption of selected species from adsorbate mixtures is prevented in resonant laser desorption in the IR due to intermolecular coupling and surface heating effects by adsorbate−surface coupling.[13] Because all adsorbed species, regardless of their structure, are affected by laser heating of the substrate, LITD is also nonselective. It is used as a standard technique for desorption of unknown analytes and analyte mixtures.[6,7]

In the literature various mechanisms have been proposed to explain the observation that thin adsorbate layers of thermally labile, polar, and nonvolatile compounds can be desorbed without fragmentation by LITD. Various authors[14−16] suggested that internally cold, intact molecules desorb if a "bottleneck" exists for energy flow from a rapidly heated surface through the surface−adsorbate bond into the internal modes of the desorbing molecules. The bottleneck for energy flow was attributed to a frequency mismatch between the low-frequency surface−adsorbate mode and the high-frequency internal vibrational modes of the adsorbed molecules. Pronounced nonthermal effects were predicted for loosely bond, physisorbed species desorbed by fast heating of the substrate.[17]

Beuhler and co-workers[18] argued that large molecules often form multiple bonds to the surfaces. Their total adsorption energy can far exceed the energy necessary for breaking one of the intramolecular bonds. Intact desorption should only occur if all of the surface−adsorbate bonds are ruptured almost simultaneously, which requires a high excess energy to be delivered to the surface−adsorbate complex. Consistent with the proposed bottleneck effect, these authors suggested that fast surface heating could prevent excitation of internal degrees of freedom of the adsorbates and therefore promote intact desorption.

Hall and De Santolo[19] as well as Deckert and George[20] suggested that fast laser heating can lead to enhanced yields of intact desorption even at a thermal equilibrium. Their explanation is based on competing desorption and decomposition channels. They argue that the process with the highest preexponential factor becomes the major reaction channel at high temperatures, regardless of the activation energy. According to Arrhenius kinetics, increased heating rates shift the temperature range at which thermal processes occur to higher values. Therefore, fast heating is expected to be beneficial for intact desorption in cases where desorption rates dominate at high temperatures. The desorption of methanol from nickel is such an example.[19] However, the effect has not been shown to be relevant for large molecules. In fact, according to transition state theory their dissociation rates are expected to dominate over desorption rates at high temperatures.[21−24]

Therefore, for elucidating LITD mechanisms and optimizing experimental techniques for intact laser desorption of large molecules, the central question concerns the heating rate at which thermal equilibrium kinetics collapse and bottleneck effects start to play a major role. In this context the Zare group[25] as well as our group[26,27] analyzed the energy partitioning on the various degrees of freedom of aniline which was laser desorbed from sapphire and silica substrates by nanosecond CO_2 laser pulses. Both groups found that the temperatures describing translation, vibration, and rotation of aniline desorbed from either substrate at heating rates on the order of 10^8-10^{10} K/s do not differ significantly. This alone can be interpreted as a result of thermal equilibrium during desorption.[25] In addition, we carried out simulations to estimate the surface temperature at which desorption occurs,[26,27] by extrapolation of temperature-programmed desorption (TPD) data obtained at much lower heating rates (<1 K/s). A surface temperature of approximately

* Author to whom correspondence should be addressed (fax: 41 1 632 12 92; e-mail: zenobi@org.chem.ethz.ch).

10.1021/jp984126i CCC: $18.00
Published on Web 02/20/1999

600 K at the time of desorption was estimated, ≈150−200 K higher than the translational and internal temperatures of the desorbed aniline. This is consistent with a bottleneck for energy flow during LITD.

The extrapolation of TPD data to the regime of laser heating rates is difficult and very sensitive to the exact shapes of the TPD curves. Therefore, we repeated the TPD experiments on the aniline/silica system with an improved experimental setup. These new results lead to a simpler interpretation of the earlier data on nanosecond laser desorption of aniline from silica[26,27] that does not require a bottleneck. Furthermore, we systematically extended the previous studies on laser desorption of aniline, which allows us to derive general conclusions on LITD mechanisms and kinetics. The new work described here includes analysis of the desorption of aniline from glassy graphite, which, in contrast to sapphire and silica, is a nonpolar substrate. Because glassy graphite absorbs at 1064 nm, we were able to perform laser desorption experiments using the fundamental of a picosecond mode-locked Nd:YAG laser. For the first time, all important kinetic parameters of one desorption system were determined experimentally: For nanosecond CO_2 laser-induced thermal desorption of aniline from glassy graphite, we measured the surface temperature transient and followed the temporal evolution of the surface coverage during the desorption process.[28] The translational energy was obtained from time-of-flight (TOF) distributions of the desorbing molecules. Vibrational and rotational temperatures were derived from resonance-enhanced multiphoton ionization (REMPI) spectra. All of these data are compared to simulations based on measured thermal equilibrium kinetic parameters.

Experimental Section

The experiments were performed in an ultrahigh vacuum (UHV) chamber described previously.[26] The surfaces, either a 20 mm × 10 mm, 3 mm thick piece of glassy graphite (Goodfellow, Cambridge, U.K.) or a 19 mm diameter, 2 mm thick disk of fused silica, both with surfaces polished to optical quality, were mounted on a manipulator to translate and rotate the sample to different ports in the UHV chamber. The substrates were in thermal contact with a liquid nitrogen reservoir for cooling. The graphite disk was heated by passing a current through the disk. The silica disk was heated by an electical current in a thin gold film that was vapor-deposited onto the back of the disk. The temperature of the substrate surfaces was measured by thermocouples cemented into holes that had been laser-drilled into the edge of the samples.

Aniline (Fluka AG, Buchs, Switzerland, specified purity ≥99.5%) was transferred into gas flasks connected to the gas handling system and degassed. The surface was dosed by leaking vapor into the chamber through a dosing system. Exposures were determined from the pressure measured by a nude ion gauge and were controlled by the exposure time (for TPD experiments) or the laser repetition rate (for LITD experiments). Surface coverages of 0.05 monolayer (ML) or lower were used in the TOF and gas phase spectroscopic experiments.

TPD experiments were performed to characterize the aniline/glassy graphite and the aniline/silica desorption systems. The substrates were heated at linear temperature rates in the range of 0.05−0.5 K/s and the partial pressure of the aniline parent ion at 93 Da was recorded on a quadrupole mass spectrometer (QMS) (Spectra Multi-Quad, Leda Mass, Stoke-on-Trent, U.K.) simultaneously with the substrate temperature. With respect to previous TPD measurements of aniline desorbing from silica,[27] the experimental setup was optimized. A microstructured dosing head was used to prevent deposition on the sample holder. Furthermore, a "Feulner cup",[29] which had previously been placed around the QMS, was removed. Both steps lead to a significant reduction of the width of the TPD peaks: decay times of TPD signals are on the order of 20 s, approximately 5 times smaller than before. TPD signals recorded with the improved QMS agree well with pressure signals which were measured using an ion gauge. This shows that broadening of the TPD signal due to the QMS is now negligible.

Two different lasers were used to induce desorption: a 70 ns CO_2 laser (Allmark 853, Alltec, Lübeck, Germany) and a 35 ps Nd:YAG laser (PY61, Continuum, Santa Clara, CA). The desorption pulses were directed onto the surface at an angle of 45°. Using apertures, we passed only the central parts of the beams onto the substrate surface. The pulse profiles on the sample had an elliptical shape with a full width at half-maximum (fwhm) of 4 mm in the horizontal direction and 3 mm in the vertical direction. The CO_2 laser fluence at the surface was determined to be 1 J/cm^2. Picosecond LITD using the Nd:YAG laser was performed at a fluence of 16 mJ/cm^2.

Surface temperature transients induced on the glassy graphite disk by nanosecond CO_2 laser heating were determined experimentally by detection of black body radiation as described in detail in ref 30. Black body radiation emitted from the heated surface was detected by a fast infrared InGaAs−PIN photodiode (model G3476-03, Hamamatsu, Herrsching, Germany). The signal was amplified by a preamplifier based on a 500 MHz operational amplifier. The emitted radiation was calibrated with measurements done at fixed surface temperatures.

Velocity distributions of laser-desorbed molecules were obtained using the same QMS as in the TPD studies. Desorbing molecules were detected in the direction of the surface normal. The flight distance from the surface to the ionization volume of the mass spectrometer was 7.5 cm. To determine exact flight time distributions with a QMS, the time response and the drift time of the ions through the instrument have to be known and the experimental data has to be deconvoluted.[31] We determined the instrumental response for aniline by pulsed extraction of residual gas, as described in ref 22 to be 80 μs, approximately three times shorter than typical TOF times.

The temporal evolution of the thin adsorbate layer during nanosecond laser desorption was followed by a novel two-laser pulse experiment in which the desorption process occurring on a nanosecond time scale is essentially transformed into TOF distributions on the microsecond time scale.[28] The desorption process initiated by the CO_2 laser was probed by pulses of a Nd:YAG laser (GCR 230, Spectra-Physics Lasers, Mountain View, CA; wavelength 1064 nm, pulse width 10 ns). For determination of the temporal evolution of the surface coverage, TOF distributions of the desorbing molecules were recorded by the QMS as a function of delay time between the two laser pulses which were overlapped at the surface. The fluences of the CO_2 laser and the Nd:YAG laser were 1 J/cm^2 and 120 mJ/cm^2, respectively.

Internal energies of laser-desorbed aniline were investigated by REMPI spectroscopy.[26,27] Molecules were desorbed either by the nanosecond CO_2 laser or the picosecond Nd:YAG laser and laser postionized in the direction of the surface normal, at the maximum of the velocity distribution. The relative contribution of the background signal stemming from ambient pressure was found to be ≈2 % and was subtracted from the spectra. The radiation of an optical parametric oscillator (MOPO-730D20, Spectra-Physics Lasers) pumped by the third harmonic of a pulsed Nd:YAG laser (GRC-230) was used for recording

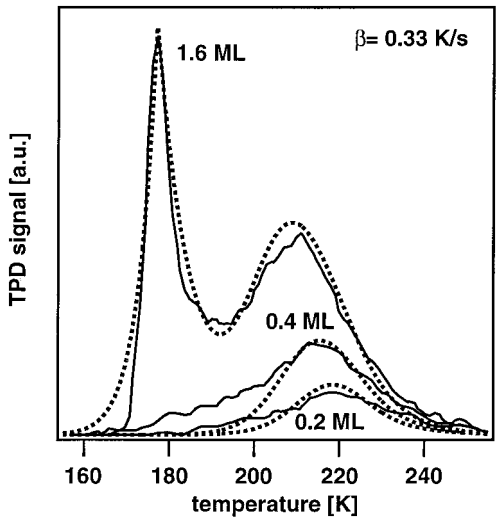

Figure 1. TPD signal of aniline adsorbate layers of various thickness desorbing from silica at a heating rate of 0.3 K/s (solid lines) and fitted desorption rates (dotted lines).

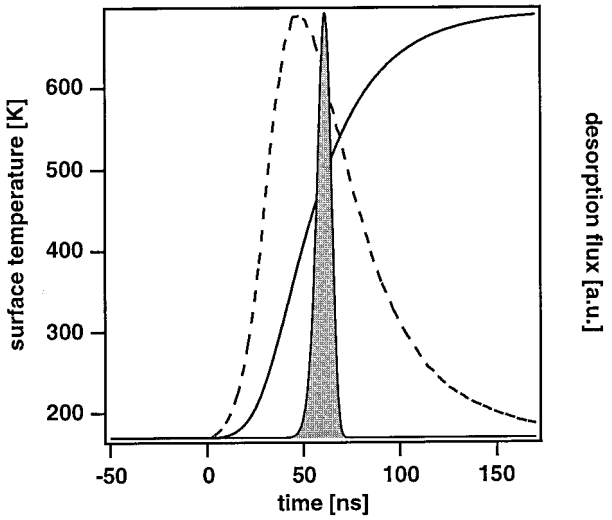

Figure 2. Measured CO_2 laser pulse profile as a function of time (dashed line), calculated surface temperature rise of the silica disk (solid line), and desorption flux of a 0.05 ML thick aniline adsorbate layer calculated on the basis of equilibrium desorption parameters ($E_A = 73$ kJ/mol; $\nu = 1.0 \times 10^{16}$ Hz) (gray shaded area).

the REMPI spectra. Saturation was avoided by the use of laser irradiances of approximately 10^4 W/cm^2. A pyroelectrical detector (ED-100, Gentec, Quebec, Canada) was placed after the ionization source to measure the energy of each UV pulse. The ions created in the REMPI process were extracted by electrical fields, mass separated in a linear TOF tube, and detected with a pair of microchannel plates. This ion signal, as well as the laser pulse energy, was integrated and averaged over 100 laser shots with two identical gated integrators and boxcar averagers (SR 250, Stanford Research Systems, Palo Alto, CA). The output at each wavelength was digitized and calibrated by dividing the ion signal by the square of the laser pulse energy.

Results

Aniline/Silica. *Thermal Equilibrium Desorption Kinetics.* Thermal equilibrium desorption kinetics were determined by fitting TPD traces using the Polanyi Wigner differential rate equation

$$\frac{d\Theta}{dt} = \Theta^n \nu \exp\left(\frac{-E_A}{kT(t)}\right)$$

where Θ is the surface coverage, n the reaction order, $T(t)$ the time-dependent surface temperature, ν the frequency factor, and E_A the activation energy. In the fits which are depicted in Figure 1, we included the broadening of the signal caused by the finite pumping rate of the vacuum chamber. At surface coverages ≤ 1 ML the TPD signal consists of a single, relatively broad peak. If the surface coverage exceeds 1 ML, a second desorption peak occurs, which is located at lower temperatures than the (sub) monolayer peak. The second peak can be attributed to desorption of molecules which do not have any direct contact to the silica substrate. When fitting TPD signals of multilayer surface coverages, we considered the two components of monolayer and multilayer desorption. The TPD peak stemming from multilayer desorption could be fitted well using zero-order kinetics with an activation energy of 59 ± 1 kJ/mol and a frequency factor of $(1 \pm 0.5) \times 10^{16}$ Hz. For submonolayer coverages best fits were obtained using first-order desorption kinetics with activation energies in the range of 70−73 kJ/mol and frequency factors of $(1 \pm 0.5) \times 10^{16}$ Hz. At all heating rates applied we found the shape and position of the submonolayer peak to be dependent on the initial coverage. At higher coverages the peak maximum is located at lower temperatures. This phenomenon might be explained by repulsive intermolecular interactions or heterogeneity of the substrate. Because the position of the desorption peak showed hardly any coverage dependence in the case of glassy graphite, we attribute the peak shift on silica to the hereogenity of the silica binding sites.

In a previous study on the desorption of benzene derivatives from silica[29] we reported that TPD traces of aniline have long tails which extend up to high temperatures. In our recent data which was recorded after we improved the experimental setup—removal of the Feulner cup which had surrounded the QMS head, and utilization of a novel dosing head—these tails no longer occurred. We interpret the tails as an experimental artifact originating from molecules which are trapped by and redesorbed from the walls of the Feulner cup before being detected by the QMS. On the basis of the data reported here, our previous findings on the equilibrium desorption kinetics of aniline from silica[29] have to be revised: the absence of the high-temperature tails in the TPD data leads to a reduction in the desorption activation energy, and a concomitant lowering of the extrapolated desorption temperature at high heating rate.

Simulations of Laser Desorption. Previous studies on CO_2 laser-induced thermal desorption of aniline surface adlayers from silica were performed at surface coverages on the order of 0.05 ML.[26,27] On the basis of the kinetic parameters given above we can extrapolate the surface temperature at which molecular desorption would be expected to occur if pure thermal equilibrium were valid under fast laser heating conditions. Figure 2 shows the measured temporal profile of the CO_2 laser. The laser-induced temperature transient on the silica surface is also depiced in Figure 2. It was calculated by numerically integrating the one-dimensional heat diffusion equation

$$\rho C_p \frac{\partial T(x,t)}{\partial t} = \frac{\partial}{\partial x}\left(k\frac{\partial T(x,t)}{\partial x}\right) + Q(x,t)$$

For comparison with previous studies, these calculations were done for the laser heating conditions applied in refs 26 and 27 (laser wavelength is 9.27 μm, fluence is 500 mJ/cm^2). For silica, the density ρ is 2.4 g/cm^3 at 300 K. In the simulations we considered the thermal dependence of the heat capacity C_p and the thermal conductivity k as given in refs 32−34. The source

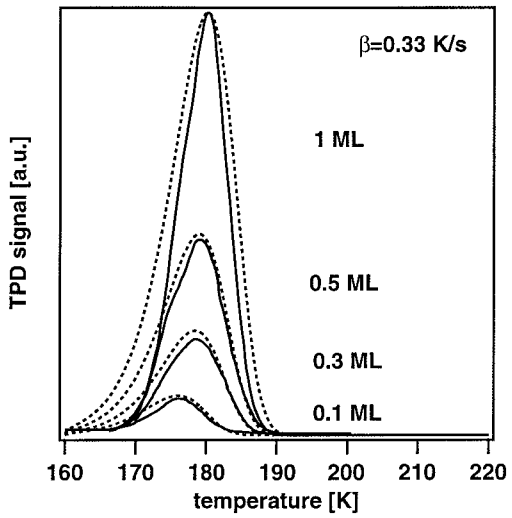

Figure 3. TPD signal of aniline adsorbate layers of various thickness desorbing from glassy graphite at a heating rate of 0.3 K/s (solid lines) and fitted desorption rates (dotted lines).

term Q takes the absorption coefficient of 3.0×10^4 cm^{-1} [35] of silica at 9.27 μm and a reflectivity of 40% into account. For the numerical integration of the heat diffusion equation the method of finite differences was used.[27,36] A time step of 1 ns and a layer thickness of 2 nm was employed, which ensured stable convergence of the procedure. The maximum surface temperature under CO_2 laser heating conditions was found to be 690 ± 50 K; the heating rate was $(5 \pm 1) \times 10^9$ K/s. The simulated trace of the desorption flux of aniline molecules which is depicted in Figure 2 was calculated by integration of the Polanyi Wigner differential rate equation for an adsorbate layer of 0.05 ML. The calculated transient surface temperature and the equilibrium desorption kinetic parameters were used in the calculations.

Given the experimental uncertainty of the activation energy and the preexponential factor, simulations varying E_A between 70 and 73 kJ/mol and ν between 0.5×10^{16} and 1.5×10^{16} Hz predict that thermal desorption of aniline should occur in the temperature range between 400 and 510 K using CO_2 laser heating, i.e., during the rising edge of the surface temperature transient. This temperature interval comprises the fwhm of the desorption traces calculated with these kinetic parameters. The temperature range is about 200 K lower than previous estimates of the desorption temperature[27,28] for the same system. An estimated desorption temperature of 400−510 K agrees well with the previously determined translational temperature of laser-desorbed aniline ($T_{kin} = 360 - 480$ K).[26,27] The ranges of the vibrational and rotational temperature ($T_{vib} = 300 - 420$ K; $T_{rot} = 250 - 450$ K) [26,27] also overlap with the calculated temperature interval; however, they are shifted toward slightly lower temperatures.

Aniline/Glassy Graphite. Graphite was used as a substrate for two reasons. First, graphite absorbs well at 10.6 μm and at 1064 nm, which allows either a CO_2 laser or the Nd:YAG laser fundamental to be used to induce thermal desorption. Second, the interaction with adsorbed molecules is weaker than in the case of silica. Bottleneck effects for energy flow from the heated substrate to the adsorbates are more likely for weakly bound adsorbates.[15,17]

Thermal Equilibrium Desorption Kinetics. Equilibrium desorption kinetic parameters were determined for the aniline/glassy graphite system by fitting TPD traces with the Polanyi Wigner equation (Figure 3). For this desorption system the components of monolayer and multilayer desorption in the TPD traces overlap completely. Monolayer and multilayer desorption therefore cannot be distinguished by the position of the TPD peaks, but only by their shapes. At low surface coverages the TPD peak is symmetric, which clearly indicates a first-order desorption process. If the surface coverage is increased, the peaks become asymmetric with a steeper slope on the high-temperature side. This peak asymmetry is typical for zero-order multilayer desorption. Best fits for submonolayer coverages were obtained using first-order desorption kinetics with activation energies in the range of 58−59 kJ/mol and a frequency factor of $(1 \pm 0.2) \times 10^{16}$ Hz. For aniline on glassy graphite, desorption of multilayers is best described by zero-order kinetics, with an activation energy of 59 ± 1 kJ/mol and a frequency factor of $(1 \pm 0.5) \times 10^{16}$ Hz.

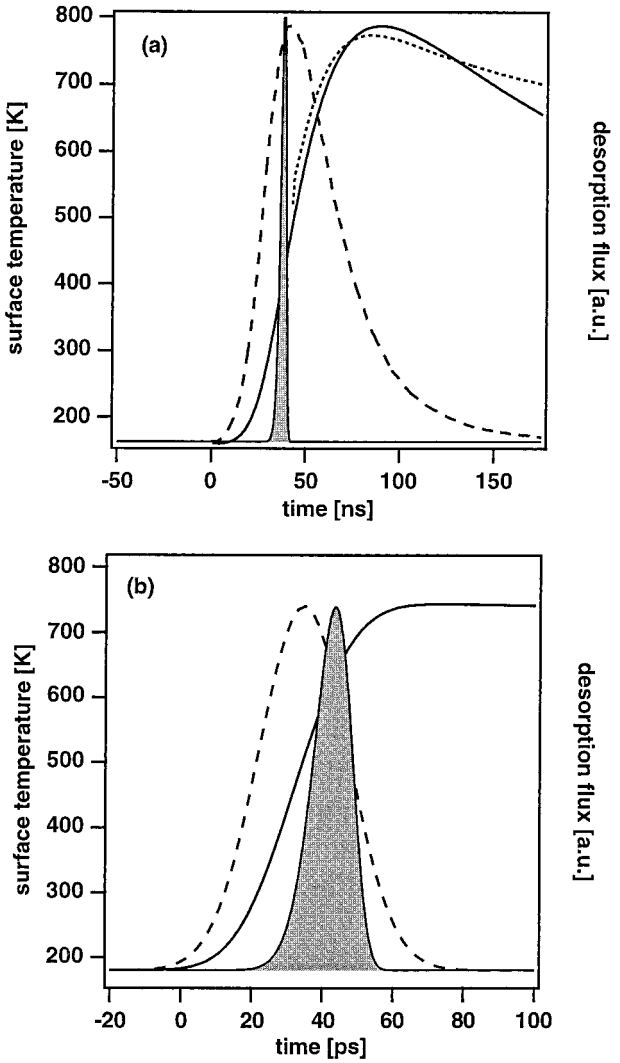

Figure 4. (a) Measured CO_2 laser pulse profile as a function of time (dashed line), calculated (solid line), and measured (dotted line) surface temperature rise of the silica disk, and desorption flux of a 0.05 ML thick aniline adsorbate layer calculated on the basis of equilibrium desorption parameters ($E_A = 58$ kJ/mol; $\nu = 1.0 \times 10^{16}$ Hz) (gray shaded area). (b) Nd:YAG laser profile (dashed line), calculated surface temperature on glassy graphite (solid line), and calculated desorption flux (gray shaded area).

Simulations of Laser Desorption. Laser-induced temperature transients on the graphite surface were calculated for nanosecond CO_2 as well as picosecond Nd:YAG laser heating by integration of the one-dimensional heat diffusion equation (Figure 4). In the simulations, we considered the thermal dependence of the

heat capacity C_p and the thermal conductivity k. The heat capacity was extracted from ref 37 by fitting the data with the Debye equation. The thermal conductivity of glassy graphite is given by $k = (3.2 \times 10^{-3})T^{1.33}$ W/(Km), where T is the temperature in Kelvin.[38,39] The density ρ of glassy graphite is 1.42 g/cm^3 at 300 K. The source term Q takes the absorption coefficient of 4.1×10^4 cm^{-1} of glassy graphite at 10.6 μm and a reflectivity of 50% into account.[40] For the numerical integration of the heat diffusion equation a layer thickness of 2 nm and time increments of 1 ns were used. The maximum surface temperature and the heating rate under CO_2 laser heating conditions were found to be 770 ± 30 K and $(1 \pm 0.2) \times 10^{10}$ K/s, respectively. The calculated temperature transient agrees well with experimental data obtained from black body radiation measurements. For picosecond Nd:YAG laser the temperature profile was calculated using the optical properties of glassy graphite at 1064 nm (reflectivity = 20%; absorption coefficient of 1.3×10^5 cm^{-1}).[40] Time increments of 1 ps were employed in this case. The simulations gave a maximum surface temperature of 740 ± 50 K and a heating rate of $(1 \pm 0.3) \times 10^{13}$ K/s.

For both laser heating scenarios the desorption flux based on thermal equilibrium desorption kinetics was calculated by integration of the Polanyi Wigner equation (Figure 4). Calculations that took the ranges of the activation energy and the preexponential factor into account predicted that desorption should occur in the temperature range of 380−450 K for nanosecond laser heating and 550−670 K for picosecond heating. This "overheating" is due to a competition between desorption and surface heating: the higher the heating rate, the higher the temperature at which desorption (or other thermal processes) will occur.[41,42]

Temporal Evolution of the Surface Coverage. We recently developed a two-pulse experiment to measure the temporal evolution of the surface coverage during laser desorption induced by 70 ns CO_2 laser pulses.[28] The experimental technique is based on the fact that the TOF distributions of aniline desorbed by the CO_2 laser (Figure 5a) and a 10 ns Nd:YAG laser, which is used as a probe, differ significantly. The surface temperature induced in the two-laser experiment follows a complex profile that depends on the time delay of the lasers. Hence, their relative timing influences the shape of the TOF distributions.

Two simple limiting cases can be identified. The TOF distribution is fast if the YAG laser pulse arrives first, because it is determined by a faster heating rate and a higher peak temperature obtained by the YAG laser. Conversely, the TOF distribution is slow if the YAG pulse arrives after the CO_2 laser pulse has completely desorbed the whole aniline layer, because of the lower heating rate of the latter. In Figure 5c the mean velocities extracted from TOF distributions recorded at various delay times between the two lasers are depicted. At a delay time of ≈50 ns after the onset of the CO_2 laser pulse, the mean velocity of desorbed molecules drops sharply from values typical for the Nd:YAG laser to values characteristic for CO_2 laser desorption. In fact, at delay times greater than 50 ns the TOF distributions are identical to those obtained by the CO_2 laser only, indicating that desorption induced by the CO_2 laser is complete after 50 ns. For the experimental conditions used, aniline completely desorbs during the rising edge of the surface temperature transient, at a surface temperature of ≈400 K. The finding is fully consistent with the desorption temperature calculated from Arrhenius type first-order desorption kinetics on the basis of equilibrium kinetic parameters (Figure 5b). The finding lends support to the notion that desorption temperatures

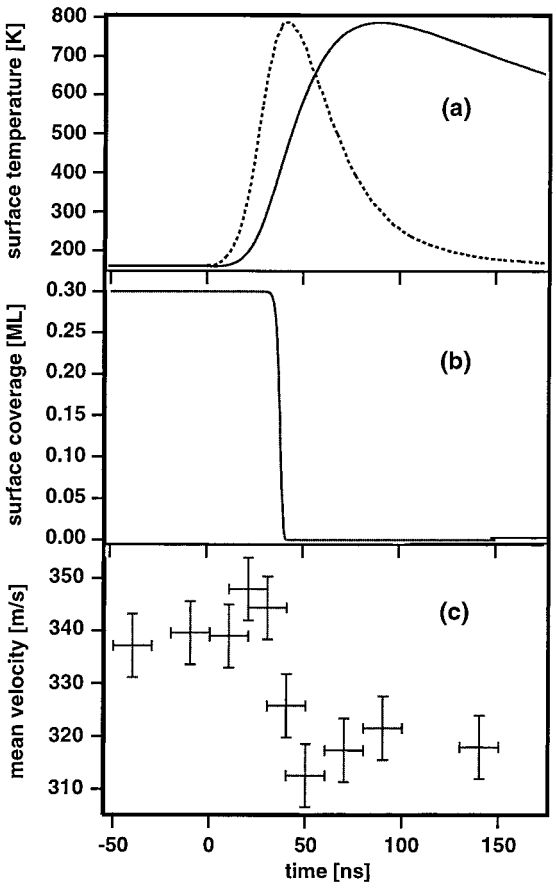

Figure 5. (a) Temporal profile of the CO_2 laser pulse (dotted line) and calculated surface temperature transient induced on the glassy graphite substrate (solid line). The origin of the time axis refers to the onset of CO_2 laser heating. (b) Calculated temporal evolution of the surface coverage assuming thermal equilibrium kinetics for the desorption of aniline from glassy graphite under CO_2 laser heating conditions. (c) Mean velocities of desorbed molecules extracted from TOF distributions recorded at various delay times between the CO_2 and the Nd:YAG laser pulses.

at laser heating rates can be obtained by extrapolation of TPD data. It also agrees well with results of Rosenzweig and Asscher[43] who found that the time at which ammonium desorbs from Re(0001) under nanosecond LITD conditions is consistent with a thermal desorption model.

Kinetic Energies of Laser-Desorbed Molecules. Translational temperatures of laser-desorbed molecules were obtained by fitting TOF distributions with Maxwell−Boltzmann (MB) distributions convoluted with the time response of the quadrupole mass spectrometer. For surface coverages of 0.05 ML the desorption plume is virtually collision-free[44,45] and no stream velocity needs to be included in the MB fits. We proved that the influence of jet effects on the TOF distributions is negligible at coverages of 0.05 ML by showing that TOF distributions within the coverage range from 0.01 to 0.1 ML have the same shape. For the fits, MB distributions of the following form were used:

$$g(t) = ct^{-4}\exp\left(-\frac{ml^2}{2kTt^2}\right)$$

where t is the flight time, m the molecular mass, T the temperature, k the Boltzmann constant, and c a constant for adjustment of the signal amplitude. The factor t^{-4} takes into account that the ionization probability of the QMS is propor-

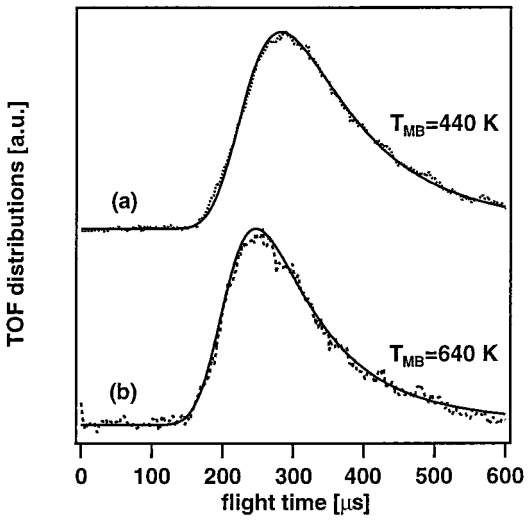

Figure 6. TOF distributions of aniline (dots) desorbed from glassy graphite by the nanosecond CO_2 laser (a) and the picosecond Nd:YAG laser (b) are depicted together with the corresponding fitted Maxwell−Boltzmann distributions (solid lines). The Maxwell−Boltzmann temperatures (T_{MB}) resulting from the fits are inserted for each trace.

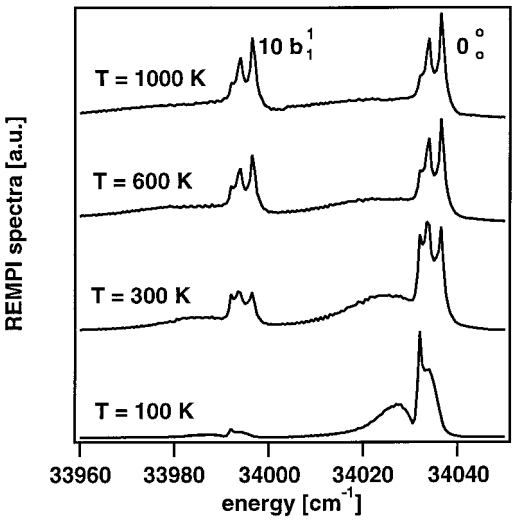

Figure 7. Computer simulations of the rotational band contour of the 0_0^0 and $10b_1^1$ transitions at various temperatures. A spectral resolution of 0.5 cm^{-1} was used in the calculations.

tional to the residence time of the molecules in the ionization volume.[31] In Figure 6, TOF distributions of aniline desorbed from glassy graphite by either the nanosecond laser or the picosecond laser are depicted together with the corresponding MB distributions. The translational temperature of molecules desorbed by the nanosecond CO_2 laser is 440 ± 50 K. Picosecond Nd:YAG laser desorption leads to kinetic temperatures of 640 ± 50 K.

Vibrational and Rotational Energies of Laser-Desorbed Molecules. In the (1 + 1) REMPI spectroscopic process aniline molecules are excited by absorption of a first photon from the electronic ground state S_0 to the first electronic state S_1 and then taken to the ionization continuum by absorption of a second photon. Because the absorption cross section for the second photon is four times higher than that for the first photon, the spectral shape of the REMPI ion signal is dominated by the absoption of the first photon. Therefore, the vibrational and rotational structure reflects the population in the electronic ground state of aniline, a prerequisite for its use as a-spectroscopic probe for internal excitation.

Vibrational and rotational excitation of the desorbed aniline molecules was studied using the the 0_0^0 origin transition and the $10b_1^1$ hot band[25] (Figure 7). In general, the relative intensity of two vibrational bands originating from levels *m* and *n* of the electronic ground state is given by

$$\frac{I_m}{I_n} = \frac{F_{i-m} g_m}{F_{j-n} g_n} \exp\left(-\frac{E_m - E_n}{kT}\right)$$

where E_m and E_n are the energies of the vibrational levels considered, T is the vibrational temperature, F_{i-m}, and F_{j-n} are the Franck−Condon factors of transitions to the vibronic states i and j, respectively. For aniline, the 10b normal mode is nondegenerate ($g_m = g_n = 1$).[46] Because the Franck−Condon factor is independent of temperature, the ratio of intensities of two transitions at two temperatures, T_1 and T_2, can be expressed by

$$\ln\left(\frac{I_m(T_1)}{I_n(T_1)}\middle/\frac{I_m(T_2)}{I_n(T_2)}\right) = \frac{\Delta E}{k}\left(\frac{1}{T_2} - \frac{1}{T_1}\right)$$

where ΔE is the difference of the energy levels, $E_m - E_n$. For the vibrational ground state and the 10b state, ΔE is 177 ± 3 cm^{-1}.[25] Therefore, on the basis of a calibration spectrum which we recorded at $T_1 = 300$ K, the vibrational temperature T_2 of laser-desorbed molecules can be determined simply by comparing the ratios of intensities of the 0_0^0 and $10b_1^1$ vibrational bands.

Rotational temperatures were determined by fitting the spectra with simulated rotational bands contours. The fitting curves were calculated with the Born−Oppenheimer and the rigid rotor approximation, using the rotational constants for aniline.[47] The resolution of the laser $\Delta\lambda$ was introduced into this calculation by assuming a Gaussian spectral profile. Each point of the spectrum is then given as a sum over all transitions considered:

$$I(E) = \sum_{\mathrm{tr}} p \cdot \exp\left(-\left(\frac{E - E_{tr}}{2\Delta\lambda}\right)^2\right)$$

where the probability p is given by

$$p = S(J'\tau';J''\tau'')\exp(-E_{J''\tau''}/kT)$$

Here $S(J'\tau';J''\tau'')$ is the Hönl−London factor expressed as a function of the total quantum number J and the index τ, which is itself related to the quantum numbers $K - 1$ and $K + 1$.[48] A total number of 300 000 transitions were taken into account for the calculations which was necessary at higher temperatures. Because the rotational envelopes obtained for the 0_0^0 and $10b_1^1$ transitions are almost identical,[49] only the 0_0^0 simulations were used for fitting the data throughout. In Figure 7 aniline spectra are depicted which were calculated for vibrational and rotational temperatures in the range of 100−1000 K.

Figure 8 shows the calibration spectrum recorded at 300 K and spectra of aniline molecules which were laser desorbed with either the nanosecond CO_2 laser or the picosecond Nd:YAG laser together with the corresponding fitted rotational contours. The vibrational and rotational temperatures resulting from the fits are inserted for each trace. To account for the spectral overlap of the two bands, the following fitting procedure was used. First, the 0_0^0 band was fitted using the main feature of only 30 cm^{-1} of the data. Then, the fit was subtracted from the measurement over the whole range, giving the deconvoluted $10b_1^1$ band, which was in turn fitted using the same, spectrally

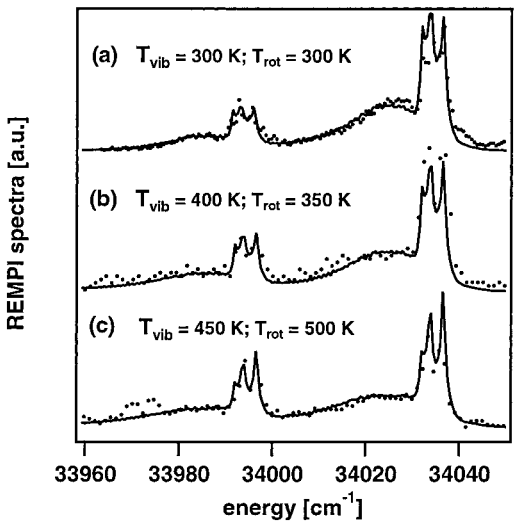

Figure 8. (a) Calibration spectrum of aniline vapor at 300 K, and spectra of (b) nanosecond CO_2 laser-desorbed and (c) picosecond Nd:YAG laser-desorbed aniline. Superimposed on the spectra are simulations of the rotational envelopes for the temperatures indicated next to the traces.

shifted band structure. The free parameter was always the relative band amplitude; an arbitrary baseline was also subtracted from the data as part of the fitting procedure. A good agreement of the fitted rotational shapes and the experimental data was obtained using rotational temperatures between 250 and 450 K for nanosecond and between 400 and 600 K for picosecond laser desorption, respectively.

At room temperature the obtained ratio of the areas of the $10b_1^1$ band and the 0_0^0 band is 0.41 ± 0.02. On the basis of the fits, the intensity ratio in the spectra was found to be in the range of 0.41−0.52 for nanosecond and 0.46−0.61 for picosecond laser desorption, corresponding to vibrational temperatures of 300−450 K and 350−600 K, respectively.

Discussion

In Table 1 the results of all experiments performed on IR LITD of aniline are summarized. With nanosecond laser heating, the temperature ranges characterizing translation, vibration, and rotation of the desorbed molecules all overlap well. These temperatures are also consistent with the calculated desorption temperatures based on equilibrium desorption kinetics.

If a bottleneck in the energy flow occurred it would be expected to be more pronounced for graphite than for silica because of the weaker substrate−adsorbate bond. However, our experimental results on nanosecond CO_2 laser desorption from graphite show that all the temperature ranges of all degrees of freedom overlap well with the calculated desorption temperature. Also, the experimentally determined surface temperature range at the time of desorption fits well into the picture of a thermal equilibrium process. On the basis of these findings, we conclude that LITD of aniline submonolayers at heating rates up to 10^{10} K/s can be fully characterized by a pure thermal equilibrium model. Pronounced bottleneck effects in the energy partitioning can certainly be ruled out on a timescale of tens of nanoseconds.

The picture is different on the time scale of tens of picoseconds. The translational temperature of aniline desorbed by the picosecond Nd:YAG laser still agrees well with the desorption temperatures extrapolated from TPD data obtained at much lower heating rates. However, the temperature ranges that characterize the vibrational and rotational excitation of the molecules are shifted toward lower temperatures.

Can collisions account for this temperature difference? For the very low surface coverages (≈0.05 ML) investigated here, an influence of collisional cooling in the desorption plume is very unlikely. Our TOF data are described well by MB distributions without an additional stream velocity term, which is a strong indication that postdesorption collisions are negligible. Typically 5−1000 collisions are required for cooling of rotational and vibrational degrees of freedom,[5] whereas significant changes of the velocity distributions are already reported for 3 collisions.[44] Recently, Elam and Levy[12] performed calculations on the effect of collisional cooling for UV laser desorption of indole. They find that typically 2−7 collisions per molecule occur after desorption of two monolayers per laser shot, resulting in only minor vibrational cooling (<10%). Therefore, the discrepancy between translational and internal temperatures found for picosecond laser heating is an indication that thermalization is not complete. These findings are consistent with the results of Heilweil et al.[50,51] on the energy flow in the other direction. These authors found that relaxation times of vibrationally excited, chemisorbed molecules are typically ≤100 ps.

With respect to mass spectrometric applications of fast LITD for volatilization of large biomolecules, one has to consider that increased internal temperatures correlate with higher fragmentation rates. Therefore, picosecond laser heating cannot generally

TABLE 1: Summary of Calculated (calc.) and Measured (meas.) Temperatures for Different Degrees of Freedom, Obtained by Nanosecond and Picosecond Laser-Induced Desorption of Aniline from Various Substrates[a]

	ns LITD from silica	ns LITD from sapphire ref 25	ns LITD from graphite	ps LITD from graphite
substrate heating rate	5×10^9 K/s (calc.)	10^8 K/s (calc.)	10^{10} K/ s (calc. and meas.)	10^{13} K/s (calc.)
surface temperature at the time of desorption	400−510 (calc.)	−	380−450 K (calc.) 350−500 K (meas.)	550−670 K (calc.)
translational energy (meas.)	360−480 K ref 27	≈400 K	380−500 K	580−700 K
vibrational energy (meas.)	300−420 K ref 27	350−550 K	300−450 K	350−600 K
rotational energy (meas.)	250−450 K ref 27	−	250−450 K	400−600 K

[a] The calculated substrate temperatures at the time of desorption refer to thermal equilibrium desorption kinetics.

be regarded as a means to enhance intact desorption. Intact desorption of nonvolatile molecules can only be expected if the bottleneck for energy flow is strong enough to compensate for the overheating associated with higher heating rates. This may become problematic for large (bio-)molecules. Recently, studies on laser-induced desorption and dissociation of poly(ethylene glycol) (PEG) submonolayers from silica were performed.[22,23] At high temperatures, dissociation rates of the PEGs clearly dominated over rates of intact desorption. The experiments showed that increasing the desorption heating rate from 1 to 10^{13} K/s leads to a reduction of the mass of the largest PEG oligomer that is still desorbed intact. This finding is also consistent with thermal equilibrium.[23] It indicates that picosecond laser heating of the PEGs does not lead to a significant reduction of the internal temperatures of the desorbing molecules.

If we generalize these findings, picosecond LITD cannot be regarded as a universal tool for intact desorption of macromolecules from surfaces. For submonolayer surface coverages, significant advantages with respect to classical heating can only be expected for desorption systems where the rates of intact desorption dominate over dissociation rates at high temperatures.[19,20] However, there is no doubt that fast laser excitation is very successful for intact desorption of thick multilayer surface coverages or matrix-embedded analyte molecules where nonthermal processes such as spallation and mechanical ablation,[52−58] as well as effective jet cooling of desorbed molecules in the desorption plume,[44,45,59−62] occur.

Summary

We carried out a systematic study on classical as well as LITD of aniline submonolayers from silica and glassy graphite. The most important conclusions from this study are (1) Nanosecond LITD of aniline from both substrates at heating rates as high as 10^{10} K/s is consistent with a thermal mechanism, i.e., the various degrees of freedom of desorbing molecules are fully thermalized and agree with the surface temperature at the time of desorption. No bottleneck for energy flow needs to be invoked. (2) At 10^{13} K/s only the kinetic energy of desorbed molecules agrees with the calculated surface temperature, whereas the internal degrees of freedom are colder. Vibrational and rotational temperatures of picosecond laser-desorbed aniline nevertheless exceed the corresponding temperatures obtained under nanosecond heating conditions. This is due to the well-known overheating caused by competing desorption and heating rates. Some restriction for energy flow clearly exists for picosecond laser desorption, but it is not strong enough to compensate for this overheating.

Acknowledgment. Our work is financially supported by the Swiss National Science Foundation (Grant 52422.97).

References and Notes

(1) Tembreull, R.; Lubman, D. M. *Anal. Chem.* **1987**, *59*, 1082.
(2) Grotemeyer, J.; Schlag, E. W. *Angew. Chem.* **1988**, *27*, 447.
(3) Karas, R.; Bahr, U.; Ingendoh, A.; Hillenkamp, F. *Angew. Chem.* **1989**, *101*, 805.
(4) Hillenkamp, F.; Karas, M.; Beavis, R. C.; Chait, B. T. *Anal. Chem.* **1991**, *63*, 1193A.
(5) Levis, R. J. *Annu. Rev. Phys. Chem.* **1994**, *45*, 483.
(6) Zenobi, R. *Chimia* **1994**, *48*, 64−71.
(7) Zenobi, R.; Zare, R. N. In *Two-Step Laser Mass Spectrometry*; Lin, S. H., Ed.; World Scientific: Singapore, 1991; pp 1−144.
(8) Voumard, P.; Zhan, Q.; Zenobi, R. *Rev. Sci. Instrum.* **1993**, *64*, 2215.
(9) Chuang, T. J.; Seki, H.; Hussla, I. *Surf. Sci.* **1985**, *158*, 525.
(10) Buck, M.; Hess, P. *Chem. Phys. Lett.* **1989**, *158*, 486.
(11) Karas, M.; Bachmann, D.; Hillenkamp, F. *Anal. Chem.* **1985**, *57*, 2935.
(12) Elam, J. W.; Levy, D. H. *J. Chem. Phys.* **1997**, *106*, 10368.
(13) Hussla, I.; Seki, H.; Chuang, T. J.; Gortel, Z. W.; Kreuzer, H. L.; Pierey, P. *Phys. Rev. B* **1985**, *32*, 3489.
(14) Lucchese, R. R.; Tully, J. C. *J. Chem. Phys.* **1984**, *81*, 6313.
(15) Zare, R. N.; Levine, R. D. *Chem. Phys. Lett.* **1987**, *136*, 593.
(16) Holme, T. A.; Levine, R. D. *Surf. Sci.* **1989**, *216*, 587−614.
(17) Zeiri, Y. *Comp. Phys. Commun.* **1994**, *80*, 200.
(18) Beuhler, R. J.; Friedman, L. *Int. J. Mass Spectrom. Ion Processes* **1987**, *78*, 1.
(19) Hall, R. B.; De Santolo, A. M. *Surf. Sci.* **1984**, *137*, 421−441.
(20) Deckert, A. A.; George, S. M. *Surf. Sci.* **1987**, *182*, 215−220.
(21) Ertl, G. In *Catalysis; Science & Technology*; Anderson, Y. R., Boudart, M., Eds.; Springer Verlag: New York, 1983; Vol. 4, pp 209−282.
(22) Handschuh, M.; Nettesheim, S.; Zenobi, R. *J. Chem. Phys.* **1997**, *107*, 2603.
(23) Handschuh, M.; Nettesheim, S.; Zenobi, R. *Chem. Phys. Lett.* **1997**, *275*, 93.
(24) Tully, J. C. *Surf. Sci.* **1994**, *299/300*, 667.
(25) Maechling, C. R.; Clemett, S. J.; Engelke, F.; Zare, R. N. *J. Chem. Phys.* **1996**, *104*, 8768.
(26) Voumard, P.; Zenobi, R.; Zhan, Q. *Surf. Sci.* **1994**, *307−309*, 360.
(27) Voumard, P.; Zenobi, R. *J. Chem. Phys.* **1995**, *103*, 6795.
(28) Handschuh, M.; Nettesheim, S.; Zenobi, R. *J. Chem. Phys.* **1998**, *108*, 6548.
(29) Voumard, P.; Zhan, Q.; Zenobi, R. *Langmuir* **1995**, *11*, 842−848.
(30) Nettesheim, S.; Zenobi, R. *Chem. Phys. Lett.* **1996**, *255*, 39.
(31) Braun, R.; Hess, P. *Int. J. Mass Spectrom. Ion Processes* **1993**, *125*, 229.
(32) Yaws, C. L. *Library of Physico-Chemical Property Data: Handbook of Thermal Conductivity*; Gulf Publishing Company: Houston, 1995.
(33) *Handbook of Chemistry and Physics, 72nd ed.*; Lide, D. R., ed.; CRC Press, Boca Raton, 1991.
(34) Parrot, J. E.; Stuckes, A. D. In *Thermal Conductivity of Solids*; Goldsmid, H. J., Ed.; Pion Limited: London, 1975, pp 123−137.
(35) Palik, E. E. *Handbook of Optical Constants of Solids*; Academic Press, Inc.: New York, 1985.
(36) Philippoz, J.-M.; Zenobi, R.; Zare, R. N. *Chem. Phys. Lett.* **1989**, *158*, 12.
(37) *Landolt-Börnstein, New Serie III/22a;* Springer, New York, 1987.
(38) Biljakovic, K.; Smontara, D.; Staresinic, D.; Pajic, D.; Kozlov, M. E.; Hirabayashi, M.; Tukomoto, M.; Ihara, H. *J. Phys.: Condens. Matter* **1996**, *8*, L27.
(39) Katerberg, J. A.; Anderson, A. C. *J. Low Temp. Phys.* **1978**, *30*, 739.
(40) Williams, M. W.; Arakawa, E. T. *J. Appl. Phys.* **1972**, *43*, 3460.
(41) Redhead, P. A. *Vacuum* **1962**, *12*, 203.
(42) Ho, W. *J. Phys. Chem.* **1996**, *100*, 13050.
(43) Rosenzweig, Z.; Asscher, M. *J. Chem. Phys.* **1992**, *96*, 4040.
(44) Kelly, R.; Dreyfus, R. W. *Surf. Sci.* **1988**, *198*, 263−276.
(45) Kelly, R.; Dreyfus, R. W. *Nucl. Instrum. Methods Phys. Res., Sect. B* **1988**, *32*, 341.
(46) Castella-Ventura, M.; Kassab, E. *Spectrochim. Acta* **1994**, *50*, 69.
(47) Christoffersen, J.; Hollas, J. M.; Kirby, G. H. *Mol. Phys.* **1969**, *16*, 441.
(48) Zare, R. N. *Angular Momentum. Understanding Spatial Aspects in Chemistry and Physics; John Wiley & Sons: New York*, 1988.
(49) Voumard, P.; Zenobi, R.; Zhan, Q. *J. Phys. Chem.* **1995**, *99*, 11722.
(50) Heilweil, E. J.; Casassa, M. P.; Cavanagh, R. R.; Stephenson, J. C. *Annu. Rev. Phys. Chem.* **1989**, *40*, 143.
(51) Beckerle, J. D.; Cavanagh, R. R.; Casassa, M. P.; Heilweil, E. J.; Stephenson, J. C. *J. Chem. Phys.* **1991**, *95*, 5403.
(52) Nelson, R. W.; Rainbow, M. J.; Lohr, D. E.; Williams, P. *Science* **1989**, *246*, 1585.
(53) Williams, P.; Nelson, R. W. In *Methods and Mechanisms for Producing Ions from Large Molecules*; Standing, K. G., Ens, W., Eds.; Plenum Press: New York, 1991; p 265.
(54) Kampmeier, J.; Dreisewerd, K.; Schürenberg, M.; Strupat, K. *Int. J. Mass Spectrom. Ion Processes* **1997**, *168/179*, 31.
(55) Haglund, J. R. F. *Appl. Surf. Sci.* **1996**, *96−98*, 1−13.
(56) Strupat, K.; Kampmeier, J.; Horneffer, V. *Int. J. Mass Spectrom. Ion Processes* **1997**, *169/170*, 43.
(57) Zhigilei, L. V.; Kodali, P. B. S.; Garrison, B. J. *J. Phys. Chem. B* **1997**, *101*, 2028.
(58) Cramer, R.; Haglund, R.; Hillenkamp, F. *Int. J. Mass Spectrom. Ion Processes* **1997**, *169/170*, 51.
(59) Vertes, A.; Irinyi, G.; Gijbels, R. *Anal. Chem.* **1993**, *65*, 2389.
(60) Cousins, L. M.; Levis, R. J.; Leone, S. R. *J. Phys. Chem.* **1989**, *93*, 5325.
(61) Cousins, L. M.; Levis, R. J.; Leone, S. R. *J. Chem. Phys.* **1989**, *91*, 5731.
(62) Elokhin, V. A.; Krutchinsky, A. N.; Ryabov, S. E. *Chem. Phys. Lett.* **1990**, *170*, 193.